Interband tunnel junctions for wurtzite III-nitride semiconductors based on heterointerface polarization charges

Martin F. Schubert
Rensselaer Nanotechnology Center, Rensselaer Polytechnic Institute, Troy, New York 12180, USA
(Received 14 October 2009; published 5 January 2010)

The concept of interband tunnel junctions for wurtzite III-Nitride semiconductors based on polarization charges at heterointerfaces is introduced. Such polarization-charge tunnel junctions obviate the need for high n-type and p-type doping, which is a general requirement for conventional tunnel junctions and also is a significant challenge for large-band-gap III-nitride semiconductors. Transmission coefficients and current-voltage characteristics for GaN/AlN/GaN and AlN/GaN/AlN polarization-charge tunnel junctions are calculated using the $k \cdot p$ quantum-transmitting boundary method with an eight-band Hamiltonian with Burt-Foreman operator ordering. It is shown that polarization-charge tunnel junctions carry sufficient current to become viable components in future light-emitting devices.

DOI: 10.1103/PhysRevB.81.035303 PACS number(s): 73.40.Gk, 73.40.Kp, 73.43.Cd, 71.15.−m

I. INTRODUCTION

The difficulty of achieving high hole concentrations in large-band-gap III-nitride semiconductors is a well-known problem. Low hole concentrations are the result of the large ionization energy of the p-type dopant Mg, which increases from approximately 120 meV in GaN (Ref. 1) to 510 meV in AlN.[2] By contrast, the activation energy for the n-type dopant Si is only 86 meV in AlN.[3] Conventional light emitters in the visible wavelength range contain layers with only low Al mole fractions, and so manage good performance despite the difficulties with p-type doping. However, current spreading in p-type layers is limited[4] and must be considered in device design to achieve favorable results.[5,6]

At emission wavelengths shorter than around 360 nm, GaN is not well suited for use as the bulk p-type material because it ceases to be transparent and its band gap provides inadequate carrier confinement. However, because of difficulties in fabricating contacts to p-type AlGaN with significant Al compositions, many experimentally realized ultraviolet (UV) light-emitting diodes (LEDs) incorporate p-type GaN contact layers together with p-type AlGaN confinement layers,[7] which harms light-extraction efficiency. Further, the low hole concentrations in p-AlGaN result in poor hole injection, and therefore reduced internal quantum efficiency;[8] the combination of low internal efficiency and poor extraction efficiency has limited the performance of the best available UV emitters to less than 1%.[7]

In principle, an interband tunnel junction can electrically couple a thin p-type layer to n-type material and eliminate the need for thick p-type regions. Conventional tunnel junctions consist of heavily doped p-n junctions; the heavy doping results in a very narrow depletion region. When the junction is biased so that the conduction band edge on the n-type side is pulled below the valence edge band on the p-type side, electrons in the valence band can tunnel into the conduction band, or equivalently, holes in the conduction band can tunnel into the valence band. Tunnel junctions have previously been investigated for GaN-based visible light emitters as current spreading layers.[9–11] However, for UV applications, such tunnel junctions would likely still be problematic due to the continued requirement of high p-type doping.

In this paper, the concept of an interband tunnel junction based on heterointerface polarization charges is introduced. The polarization-charge tunnel junction exploits contrast in material polarization among III-nitride semiconductors to achieve very short tunneling distances without the need for high doping concentrations. Section II discusses polarization in III-nitrides and treats the design of polarization-charge tunnel junctions in detail. The transmission coefficients and current-voltage characteristics of tunnel junctions are modeled by the $k \cdot p$ multiband quantum-transmitting boundary method (MQTBM) (Ref. 12) using an eight-band Hamiltonian for wurtzite materials with Burt-Foreman operator ordering.[13,14] Section III presents the Hamiltonian, together with a brief description of the MQTBM and the method for calculating the electrostatic potential in the tunnel junction, as well as some limitations of the present approach. In Section IV, calculation results for several tunnel junctions are presented and discussed in detail. Finally, a summary is given in Section V.

II. POLARIZATION-CHARGE TUNNEL JUNCTION DESIGN

The polarization-charge tunnel junction concept takes advantage of material polarization, which is inherent in wurtzite III-nitride semiconductors.[16] Total polarization in a layer consists of spontaneous polarization P_{sp}, which depends upon the material composition, and the piezoelectric polarization P_{pz}, which appears when there is strain in the layer. For the case of heterostructures grown in the c direction, strain is given by

$$\varepsilon_{xx} = \varepsilon_{yy} = \frac{a_{sub} - a}{a}, \tag{1}$$

$$\varepsilon_{zz} = -2\frac{C_{13}}{C_{33}}\varepsilon_{xx}, \tag{2}$$

 ©2010 The American Physical Society

TABLE I. Polarization-related material parameters (Ref. 17). For alloy material parameters, linear interpolation is used except for those with bowing parameters listed in Table II.

Parameter	AlN	GaN
Spontaneous polarization ($C\ m^{-2}$)		
P_{sp}	−0.090	−0.034
Lattice constant (Å)		
a	3.112	3.189
Piezoelectric coefficient ($pm\ V^{-1}$)		
d_{13}	−2.1	−1.0
Elastic constants (GPa)		
C_{11}	396	390
C_{12}	137	145
C_{13}	108	106
C_{33}	373	398

and nondiagonal components of the strain tensor vanish. The piezoelectric polarization is oriented along the growth direction and is given by

$$P_{pz} = \varepsilon_{xx} 2 d_{13}\left(C_{11} + C_{12} - \frac{2C_{13}^2}{C_{33}}\right). \quad (3)$$

Material parameters used in calculation of polarization are shown in Table I. At heterointerfaces of structures grown in the c direction, there is discontinuity in polarization which gives rise to sheet charges at the interfaces. In a double heterostructure, equal and opposite sheet charges appear at the two interfaces, and produce a strong electric field and large potential drop across the intermediate layer. This explains the quantum-confined Stark effect observed in GaInN/GaN quantum wells.[18]

The polarization-charge tunnel junction is exactly such a double heterostructure, with the intermediate layer thickness chosen so that the potential drop across it is equal to the band gap of the surrounding layers—just like a the potential drop in the depletion region in a conventional tunnel junction. In effect, the polarization-charge tunnel junction is just like a conventional tunnel junction except that charges in the depletion region resulting from ionized acceptors and donors are replaced by sheet charges resulting from polarization mismatch. The polarization of the n-type and p-type layers which are joined by the tunnel junction determines what materials can be used as the tunneling layer as well as the position of the tunnel junction within the device—i.e., above or below the p-type region.

TABLE II. Nonzero bowing parameters (Ref. 17).

Parameter	AlGaN
Band gap (eV)	
E_g	0.8
Spontaneous polarization ($C\ m^{-2}$)	
P_{sp}	−0.021

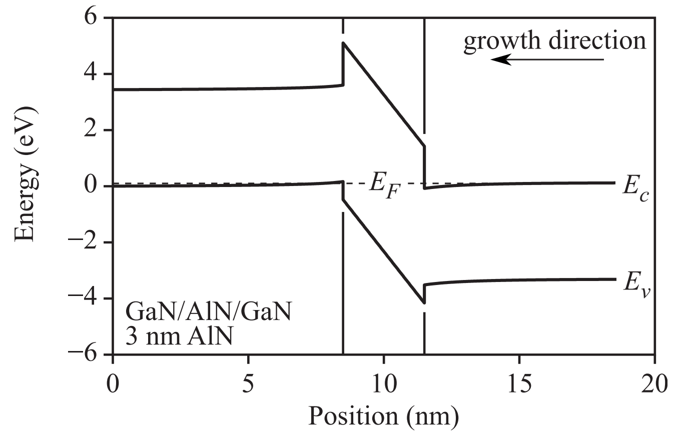

FIG. 1. Calculated band diagram of a GaN/AlN/GaN polarization-charge tunnel junction with a 3 nm AlN layer.

One possible polarization-charge tunnel junction structure consists of an intermediate AlN layer sandwiched between GaN layers. When this structure is grown pseudomorphically on the metal face of a GaN template, a positive sheet charge exists on the nitrogen face of the AlN layer while a negative sheet charge exists on the metal face. As a result of this charge arrangement, there is an induced hole concentration above the tunnel junction, and therefore the appropriate position for the tunnel junction is below the p-type region (assuming a bottom n-type template). Figure 1 shows the calculated band diagram of a GaN/AlN/GaN tunnel junction. The AlN layer is 3 nm thick, which is slightly larger than needed to yield a potential drop equal to the built-in voltage between the n-type and p-type layers, and causes carriers to accumulate at its edges.

Alternatively, when an AlN/GaN/AlN heterostructure is grown pseudomorphically on the metal face of an AlN

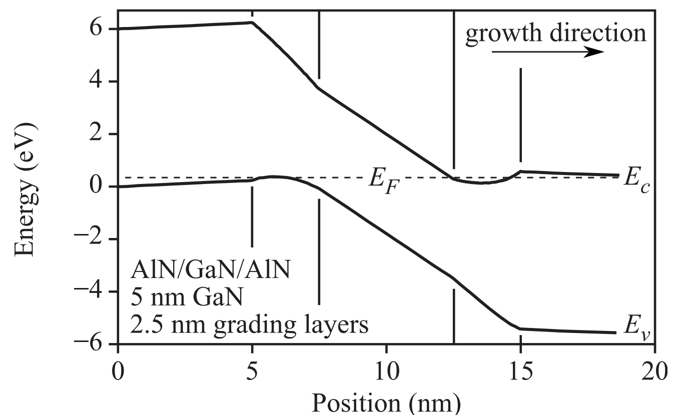

FIG. 2. Calculated band diagram of a AlN/GaN/AlN polarization-charge tunnel junction with a 5 nm GaN layer. At the interfaces, the alloy composition is linearly graded over a 2.5 nm distance.

template, a positive sheet charge exists on the metal face of the GaN layer, while a negative sheet charge exists on the nitrogen face. This charge arrangement is opposite of the GaN/AlN/GaN tunnel junction, and therefore, in a device the junction would be located above the p-type region. In a pure AlN/GaN/AlN junction, however, the larger bandgap of AlN compared to GaN results in depletion of AlN. Depletion of electrons in n-type AlN on the metal face of GaN occurs because the conduction band of GaN is pinned at the Fermi level; due to its larger band gap, the conduction band of the adjacent AlN will necessarily be more distant from the Fermi level, resulting in low electron concentrations. The same is true for holes on the opposite side of the junction. Therefore, a graded transition from GaN to AlN on both sides of the junction would be advantageous. Figure 2 shows the calculated band diagram of an AlN/GaN/AlN with linearly graded interfaces.

Compositional grading the interfaces has the effect of distributing the polarization charge over a volume. The high polarization charge density attracts high concentrations of free carriers. As seen in Fig. 2, on the two sides of the junction, the band edges are pushed very close to the Fermi level. In these regions, carrier density is extremely high, and is calculated to be above 10^{20} cm^{-3} for both electrons and holes, which could be advantageous for device performance.

III. METHODS

In the following subsections, the method of calculating current flowing through polarization-charge tunnel junctions is detailed. The calculation of electrostatic potential and band diagrams of tunnel junctions under bias is described first, followed by presentation of the $k\cdot p$ Hamiltonian. Next, the MQTBM is briefly outlined, followed by description of the calculation of total current flowing through the junction. Finally, some limitations of the approach are discussed.

A. Calculation of potential

The electrostatic potential ϕ within a tunnel junction is calculated by one-dimensional solution of Poisson's equation including material polarization,

$$\frac{\partial}{\partial z}\left(-\varepsilon\frac{\partial}{\partial z}\phi + P_{sp} + P_{tot}\right) = \rho, \tag{4}$$

where ε is the dielectric constant, ρ is the charge due to electrons, holes, and ionized dopants, and the z direction is the growth direction and is parallel to the c axis. Under electrical bias, Eq. (4) is solved self-consistently with the continuity equations for electrons and holes,

$$\frac{\partial}{\partial z}\left(n\mu_n\frac{\partial}{\partial z}E_{Fn}\right) - qR = 0, \tag{5}$$

$$\frac{\partial}{\partial z}\left(p\mu_p\frac{\partial}{\partial z}E_{Fp}\right) + qR = 0, \tag{6}$$

where n and p are the electron and hole concentrations, μ_n and μ_p are the electron and hole mobilities, E_{Fn} and E_{Fp} are the quasi-Fermi levels, and R is the recombination rate. Equations are discretized using the box integration method.[19] Carrier densities are calculated using Fermi statistics assuming parabolic bands with effective masses calculated from the eight-band Hamiltonian described in the following section. The offset in the conduction band at a heterointerface is assumed to be 70% of the total band-gap difference. For the bias voltages considered, the classical solution of Eqs. (4)–(6) results in negligible current and recombination, and so the final potential is not dependent on the mobilities.

B. $k\cdot p$ Hamiltonian definition

The derivation of the Hamiltonian starts from the approximate local form of the exact envelope-function equations.[13] Following Foreman[14] the equations are simplified yielding a Hamiltonian with unambiguous operator ordering for the valence band that ensures Hermiticity. This process does not give specific operator ordering for matrix elements coupling conduction and valence bands; for these terms, ordering is chosen as in Ref. 15. In the basis

$$|1\rangle = |iS\uparrow\rangle,$$

$$|2\rangle = |iS\downarrow\rangle,$$

$$|3\rangle = -1/\sqrt{2}|(X+iY)\uparrow\rangle,$$

$$|4\rangle = +1/\sqrt{2}|(X-iY)\uparrow\rangle,$$

$$|5\rangle = |Z\uparrow\rangle,$$

$$|6\rangle = +1/\sqrt{2}|(X-iY)\downarrow\rangle,$$

$$|7\rangle = -1/\sqrt{2}|(X+iY)\downarrow\rangle,$$

$$|8\rangle = |Z\downarrow\rangle, \tag{7}$$

the resulting $k\cdot p$ Hamiltonian for growth along the c axis is given by

$$H = \begin{bmatrix} E_c & 0 & -P_2\hat{k}_+/\sqrt{2} & P_2\hat{k}_-/\sqrt{2} & P_1\hat{k}_z & 0 & 0 & 0 \\ 0 & E_c & 0 & 0 & 0 & P_2\hat{k}_-/\sqrt{2} & -P_2\hat{k}_+/\sqrt{2} & P_1\hat{k}_z \\ -P_2\hat{k}_-/\sqrt{2} & 0 & F-\rho & -K^* & -H_+^* & 0 & 0 & 0 \\ P_2\hat{k}_+/\sqrt{2} & 0 & -K & G+\rho & H_+ & 0 & 0 & \sqrt{2}\Delta_2 \\ P_1\hat{k}_z & 0 & -H_- & H_-^* & \lambda & 0 & \sqrt{2}\Delta_2 & 0 \\ 0 & P_2\hat{k}_+/\sqrt{2} & 0 & 0 & 0 & F+\rho & -K & H_+ \\ 0 & -P_2\hat{k}_-/\sqrt{2} & 0 & 0 & \sqrt{2}\Delta_2 & -K^* & G-\rho & -H_+^* \\ 0 & P_1\hat{k}_z & 0 & \sqrt{2}\Delta_2 & 0 & -H_-^* & -H_- & \lambda \end{bmatrix} \quad (8)$$

where the following definitions are used:

$$E_c = E_g + E_v^{\max} + \hat{k}_x\frac{\hbar^2}{2\tilde{m}_e^{\parallel}}\hat{k}_x + \hat{k}_y\frac{\hbar^2}{2\tilde{m}_e^{\parallel}}\hat{k}_y + \hat{k}_z\frac{\hbar^2}{2\tilde{m}_e^{\perp}}\hat{k}_z,$$

$$F = \lambda + \theta + \Delta_1 + \Delta_2,$$

$$G = \lambda + \theta + \Delta_1 - \Delta_2,$$

$$\lambda = \frac{\hbar^2}{2m_0}(\hat{k}_z\tilde{A}_1\hat{k}_z + \hat{k}_x\tilde{A}_2\hat{k}_x + \hat{k}_y\tilde{A}_2\hat{k}_y) + \lambda_\varepsilon,$$

$$\theta = \frac{\hbar^2}{2m_0}(\hat{k}_z\tilde{A}_3\hat{k}_z + \hat{k}_x\tilde{A}_4\hat{k}_x + \hat{k}_y\tilde{A}_4\hat{k}_y) + \theta_\varepsilon,$$

$$\rho = \frac{\hbar^2}{2m_0}[i\hat{k}_y(\tilde{A}_5^+ - \tilde{A}_5^-)\hat{k}_x - i\hat{k}_x(\tilde{A}_5^+ - \tilde{A}_5^-)\hat{k}_y],$$

$$K = \frac{\hbar^2}{2m_0}(\hat{k}_x\tilde{A}_5\hat{x}_z - \hat{k}_y\tilde{A}_5\hat{k}_y + i\hat{k}_x\tilde{A}_1\hat{k}_y + i\hat{k}_y\tilde{A}_1\hat{k}_x),$$

$$H_\pm = \frac{\hbar^2}{2m_0}(\hat{k}_+\tilde{A}_6^\pm\hat{k}_z + \hat{k}_z\tilde{A}_6^\mp\hat{k}_+),$$

$$\hat{k}_\pm = \hat{k}_x \pm i\hat{k}_y,$$

$$\lambda_\varepsilon = D_1\varepsilon_{zz} + D_2(\varepsilon_{xx} + \varepsilon_{yy}),$$

$$\theta_\varepsilon = D_3\varepsilon_{zz} + D_4(\varepsilon_{xx} + \varepsilon_{yy}),$$

$$\Delta_\varepsilon = a_1\varepsilon_{zz} + a_2(\varepsilon_{xx} + \varepsilon_{yy}). \quad (9)$$

Here, $E_v^{\max}$ is the valence band maximum taking into account strain, and P_1 and P_2 are the Kane's parameters derived in Ref. 21. All material parameters in Eq. (9) are taken to be position dependent. In bulk, the operator $\hat{k}_\alpha$ commutes with material parameters, and the Hamiltonian (8) is equivalent to that of Ref. 20, with the exception that the cubic approximation is not used here. In heterostructures, where translational invariance is relaxed, the terms arising from asymmetric splitting of the parameters $\tilde{A}_5$ and $\tilde{A}_6$ are an additional difference.[22]

Material parameters for III-nitride are commonly specified for use in a 6×6 Hamiltonian for the valence bands, and a single-band Hamiltonian for the conduction band; these are shown in Table III. The parameters in Table III already contain the influence of conduction upon valence bands and valence upon conduction band perturbatively. Since Eq. (8) treats all bands explicitly, the coupling must be removed. The modified effective masses (lying in the c plane and perpendicular to it) are related to those in Table III by

$$\tilde{m}_e^{\parallel} = \left(\frac{1}{m_e^{\parallel}} - \frac{2}{\hbar^2}\frac{P_2^2}{E_g}\right)^{-1},$$

$$\tilde{m}_e^{\perp} = \left(\frac{1}{m_e^{\perp}} - \frac{2}{\hbar^2}\frac{P_1^2}{E_g}\right)^{-1}. \quad (10)$$

The modified valence band parameters are given by

$$\tilde{A}_1 = A_1 + \frac{2m_0}{\hbar^2}\frac{P_1^2}{E_g},$$

$$\tilde{A}_2 = A_2 - \frac{2m_0}{\hbar^2}\frac{P_1^2}{E_g},$$

$$\tilde{A}_4 = A_4 + \frac{m_0}{\hbar^2}\frac{P_2^2}{E_g},$$

$$\tilde{A}_5^+ = A_5^+ + \frac{m_0}{\hbar^2}\frac{P_2^2}{E_g},$$

$$\tilde{A}_6^+ = A_6^+ + \frac{\sqrt{2}m_0}{\hbar^2}\frac{P_1P_2}{E_g}, \quad (11)$$

and the remaining valence band parameters are unchanged. Following ellipticity arguments by Veprek *et al.*,[22] we let $A_5^- = A_6^- = 0$.

TABLE III. Material parameters (Ref. 17). For alloy material parameters, linear interpolation is used except for those with bowing parameters listed in Table II.

Parameter	AlN	GaN
Band gap (eV)		
E_g	6.00	3.437
Crystal field splitting (eV)		
$\Delta_{cr}=\Delta_1$	−0.227	0.0104
Spin orbit splitting (eV)		
$\Delta_{so}=3\Delta_2$	0.017	0.036
Electron effective mass (m_0)		
$m_e^{\parallel}$	0.32	0.21
$m_e^{\perp}$	0.30	0.20
Valence band A parameters		
A_1	−3.86	−7.21
A_2	−0.25	−0.44
A_3	3.58	6.68
A_4	−1.32	−3.46
A_5	−1.47	−3.40
A_6	−1.64	−4.90
Interband deformation potential (eV)		
a_1	−3.4	−7.1
a_2	−11.8	−9.9
Valence band deformation potential (eV)		
D_1	−2.9	−3.6
D_2	4.9	1.7
D_3	9.4	5.2
D_4	−4.0	−2.7
D_5	−3.3	−2.8
D_6	−2.7	−4.3

C. $k\cdot p$ multiband quantum-transmitting boundary method

Transmission coefficients for tunnel junctions are calculated using the MQTBM as formulated for the $k\cdot p$ method.[12] This approach reduces the problem to a calculation of the energy eigenstates for a system consisting of the tunnel junction in the center, and semi-infinite bulk regions to either side, each with potential and composition matching the respective end point of the tunnel junction.

The wave function is described by a spatially varying vector F, whose elements are the coefficients of the basis (7). Within the tunnel junction, where the potential and material parameters are position dependent, the wave function corresponding to a particular energy E, k_x, and k_y satisfies

$$HF - EF = 0 \tag{12}$$

with the substitution in $H(\hat{k}_z \rightarrow -id/dz)$. This forms a set of coupled differential equations which is discretized using the box integration method, leaving a finite set of linear equations which can be solved to find F at each grid point provided that F is known at the end points.

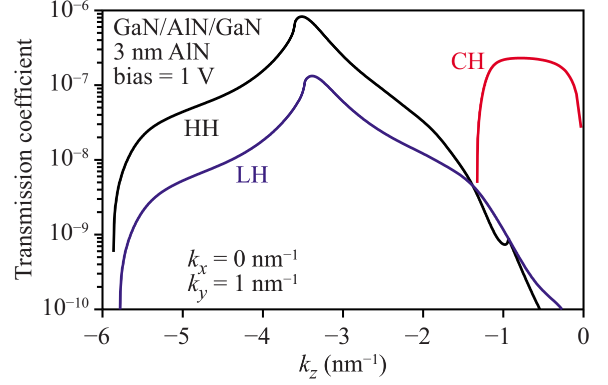

FIG. 3. (Color online) Transmission as a function of k_z for a GaN/AlN/GaN polarization-charge tunnel junction.

In the semi-infinite bulk regions, the solutions of Eq. (12) include Bloch plane-wave solutions, for which F can be written as

$$F_k(x,y,z) = C_k \exp[i(k_x x + k_y y + k_z z)], \tag{13}$$

where C_k is a vector of coefficients of the basis states, and is position independent. In general, for given E, k_x, and k_y, since the Hamiltonian for the bulk can be written as

$$H(k_x,k_y,k_z) = H_2 k_z^2 + H_1(k_x,k_y)k_z + H_0(k_x,k_y) \tag{14}$$

there are twice as many (C_k, k_z) pairs which satisfy Eq. (12) as there are bands represented in H. These pairs can be found by solving the eigenvalue problem,[23,24]

$$\begin{bmatrix} 0 & 1 \\ -(H_2)^{-1}(H_0 - E) & -(H_2)^{-1}H_1 \end{bmatrix} \begin{bmatrix} C_k \\ k_z C_k \end{bmatrix} = k_z \begin{bmatrix} C_k \\ k_z C_k \end{bmatrix}.$$

The current carried by a particular solution is[12,25]

$$J_z = \frac{1}{i\hbar}(2ik_z C_k^\dagger H_2 C_k + iC_k^\dagger H_1 C_k). \tag{15}$$

Solutions are grouped into right-going states which either carry current or decay in amplitude to the right, and left-going states, which carry current or decay to the left. Due to the complicated curvature of the valence bands and the inclusion of conduction bands, no general relationship between

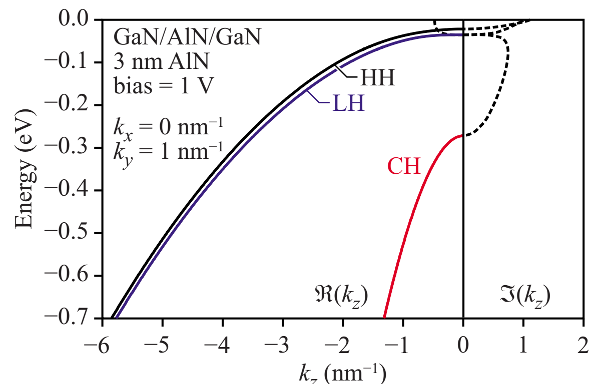

FIG. 4. (Color online) Complex valence band structure corresponding to the transmission curves in Fig. 3.

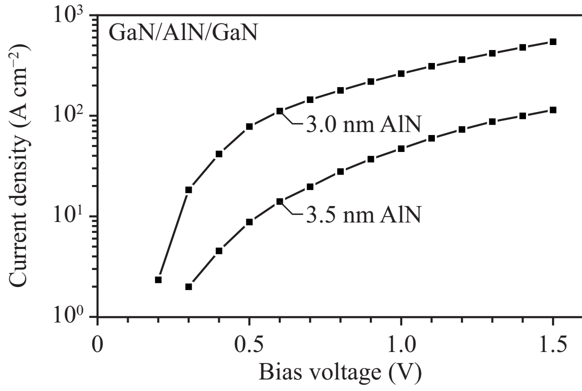

FIG. 5. Current-voltage characteristics of GaN/AlN/GaN tunnel junctions with 3.0 and 3.5 nm AlN layer thickness.

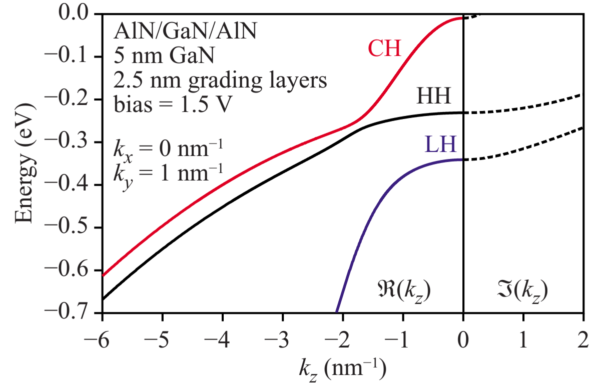

FIG. 7. (Color online) Complex valence band structure corresponding to the transmission curves in Fig. 6.

the sign of k_z and the direction of current holds.

On the left boundary of the junction, the wave function is expressed as the sum of a particular current-carrying right-going state, and a linear combination of reflected left-going states, each with unknown amplitude r_j. On the right boundary of the junction, the wave function is expressed as a linear combination of transmitted right-going states, each with unknown amplitude t_j. The z dependence of each of the states in these expansions is given by Eq. (13), and so expressions for the wave function at a point beyond the left boundary, and a point beyond the right boundary are easily found.

Using expressions for the wave function at nearby points within the semi-infinite bulk regions, the unknowns r_j and t_j can be eliminated. These equations then naturally couple to the discretized form of Eq. (12). The details of this coupling, and the final calculation of the transmission coefficient T for a particular incident Bloch plane wave, are described in Ref. 12.

D. Evaluation of total current

The total tunneling current is given by

$$J = \frac{q}{8\pi^3}\sum_j \int_{\Omega_j} (f_L - f_R) T_j v_{z,j} d^3k, \tag{16}$$

where the sum is over all right-going current-carrying Bloch plane-waves on the left side of the tunnel junction, T_j is the k-dependent transmission coefficient of the jth plane wave, $v_{z,j}$ is its group velocity, and f_L and f_R is the Fermi distribution function evaluated to the left and right of the junction. The integration domain Ω_j contains the entire volume of momentum space which corresponds to Bloch plane waves that carry current to the right.

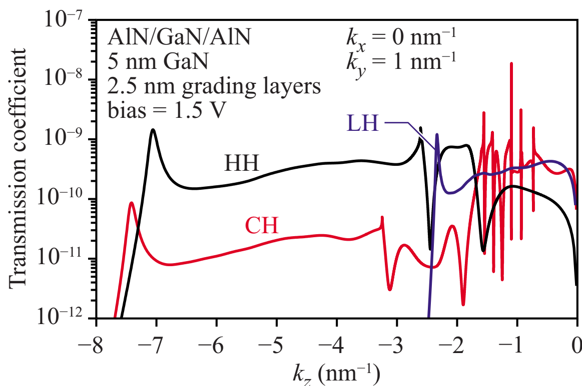

FIG. 6. (Color online) Transmission as a function of k_z for an AlN/GaN/AlN polarization-charge tunnel junction.

E. Limitations of the present approach

The MQTBM is used here to evaluate the total current due to tunneling between extended states on the two sides of the junction. As seen in Figs. 1 and 2, the conduction band on the left and valence band on the right do not overlap at zero applied bias, and so there will be a threshold for tunneling by extended states to occur. However, in both cases, there exist potential wells on each side of the junction: a well for electrons on the n-type side, and a well for holes on the p-type side. Within the wells, there is overlap of conduction and valence bands. Therefore, the polarization charge could operate as a form of resonant interband tunnel diode,[26] wherein current flows due to tunneling between bound states.

Further, in this work, electronic states within the band gap of the tunnel barrier are not considered; such electronic states can be caused by native defects as well as dopants or unwanted impurities. Electronic states in the gap can increase the tunneling current by a significant amount, and consideration of such states is critical to increasing the accuracy of theoretically calculated tunneling currents.[27] Even with the inclusion of states in the band gap, however, the theoretically calculated tunneling current is generally less than the experimentally observed value.[27] For these reasons, experimentally observed tunneling currents for polarization-charge tunnel junctions are expected to exceed those calculated in this work, particularly at lower bias voltages.

IV. RESULTS AND DISCUSSION

Figure 3 shows the transmission coefficient through a GaN/AlN/GaN polarization-charge tunnel junction with 3 nm AlN thickness under 1 V bias and with $k_y = 1$ nm^{-1}. The associated complex valence band structure is shown in Fig. 4. The transmission coefficient is characterized by a complex shape including several peaks; peaks for transmission for the

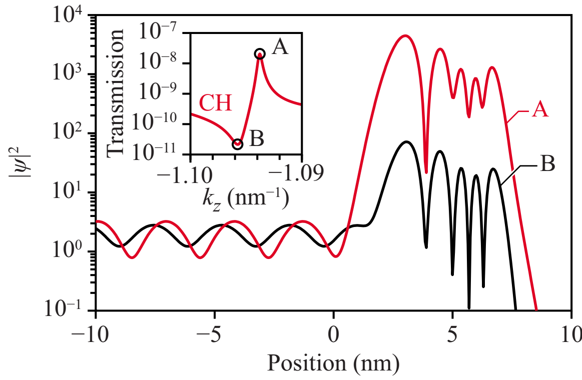

FIG. 8. (Color online) Wave functions in an AlN/GaN/AlN tunnel junction in the vicinity of a resonance in transmission coefficient. Inset shows a magnified view of the transmission curve from Fig. 6.

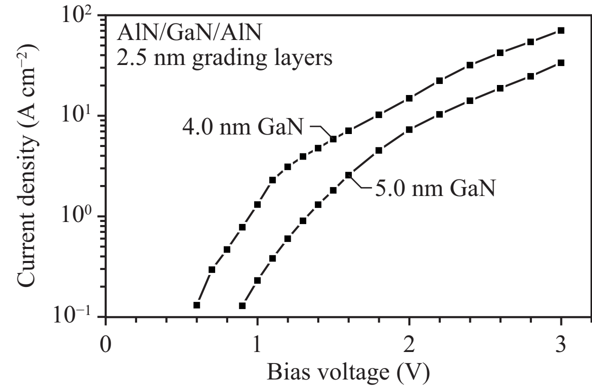

FIG. 9. Current-voltage characteristics of AlN/GaN/AlN tunnel junctions with 4.0 and 5.0 nm GaN layer thickness. The interfaces between AlN and GaN are graded over 2.5 nm.

heavy hole (HH) band correspond to k_z values where the energy of the HH band match the maxima of the light hole (LH) or crystal hole (CH) band. Similarly, the LH band has a transmission peak at the k_z value where its energy matches the maximum of the CH band. Such peaks in transmission are generally present, but vary with the in-plane k vector, applied voltage, and the thickness of the AlN layer.

Due to its large group velocity—evidenced by strong curvature in Fig. 4—and its relatively high transmission coefficient, the majority of current in the GaN/AlN/GaN polarization-charge tunnel junction is due to tunneling from incident plane waves in the crystal hole band. Evaluating the triple integral (16) to find the total current is computationally expensive, and so rotational symmetry is assumed in the $k_x - k_y$ plane. The total current is shown in Fig. 5 as a function of the applied bias for polarization-charge tunnel junctions with 3 and 3.5 nm AlN thickness. For the junction with 3 nm AlN thickness, the current at only 0.5 V bias reaches nearly 100 A cm^{-2}, which is sufficient for devices such as high-power LEDs.

The transmission coefficient through an AlN/GaN/AlN polarization-charge tunnel junction is shown in Fig. 6 for $k_y = 1$ nm^{-1} and a bias voltage of 1.5 V. The AlN layer thickness is 5 nm, and the interface between GaN and AlN is linearly graded over 2.5 nm on both sides of the junction. The transmission coefficient features a large number of peaks and resonances which are not directly correlated with the bulk valence band structure, which is shown in Fig. 7. Rather, the details of the potential within the tunnel junction play an important role.

The inset in Fig. 8 plots the transmission coefficient for incident CH Bloch plane-wave solutions over a narrow range in k_z where the transmission shown in Fig. 6 varies extremely rapidly. The wave functions at the peak of transmission and the minimum are shown in Fig. 8. The maximum value of $F^{\dagger}F$ for the k_z value yielding maximum transmission is more than 50 times greater than the value of $F^{\dagger}F$ for the k_z value yielding minimum transmission.

The increased amplitude for the wave function arises due to the presence of a potential well for carriers induced by the polarization charge, as seen in Fig. 2. When the incident Bloch plane wave is resonant with the well, a large amplitude for the wave function develops as a result of constructive interference, leading to a large transmission coefficient. When the incident plane wave is antiresonant, destructive interference drives the transmission coefficient down. These resonances in potential wells are the origin of the rapid variation of transmissivity seen in Fig. 6. The difference in transmission resulting from this effect can be as high as 10^4 over a relatively small change k_z. Varying the structure of the tunnel junction—by modifying the graded interfaces, or changing the GaN thickness—affects the shape of the potential wells, and changes the location and magnitude of the resonances. In a GaN/AlN/GaN polarization-charge tunnel junction, changing the AlN thickness will similarly affect the transmission coefficient.

Tunneling current through the AlN/GaN/AlN polarization-charge tunnel junction is shown as a function of voltage in Fig. 9. Due to the larger band gap of AlN compared to GaN, the tunneling length is increased, which reduces the current at a given applied voltage. However, at moderate bias voltages the tunnel junction reach currents in excess of 10 A cm^{-2}. Such currents are already suitable for devices with lower current density. However, as mentioned earlier, experimentally observed currents are expected to significantly exceed those calculated in this work, and so even AlN/GaN/AlN polarization-charge tunnel junctions may prove viable for high-power applications.

V. SUMMARY

Polarization-charge tunnel junctions for wurtzite III-nitride semiconductors have been introduced and modeled using the $k \cdot p$ multiband quantum-transmitting boundary method (MQTBM). Such tunnel junctions make use of sheet charges that arise from polarization mismatch at heterointerfaces perpendicular to the c axis to achieve large potential drops over extremely short distances. Polarization-charge tunnel junctions eliminate the need for heavy doping, which

is a requirement for conventional tunnel junctions, and a significant challenge for large-band-gap III-nitride devices. Simulation results indicate that the polarization-charge tunnel junctions carry sufficient current to be useful components in future devices.

ACKNOWLEDGMENTS

This material is based upon work supported by the National Science Foundation under Grant No. DMR-0642573 and by NYSTAR under Contract No. C070119.

[1] V. Bougrov, M. E. Levinshtein, S. L. Rumyantsev, and A. Zubrilov, in *Properties of Advanced Semiconductor Materials: GaN, AlN, InN, BN, SiC, SiGe*, edited by M. E. Levinshtein, S. L. Rumyantsev, and M. S. Shur (Wiley, New York, 2001), pp. 1–30.

[2] K. B. Nam, M. K. Nakarmi, J. Li, J. Y. Lin, and H. X. Jiang, Appl. Phys. Lett. **83**, 878 (2003).

[3] Y. Taniyasu, M. Kasu, and N. Kobayashi, Appl. Phys. Lett. **81**, 1255 (2002).

[4] X. Guo and E. F. Schubert, Appl. Phys. Lett. **78**, 3337 (2001).

[5] X. A. Cao and S. D. Arthur, Appl. Phys. Lett. **85**, 3971 (2004).

[6] D. W. Kim, H. Y. Lee, M. C. Yoo, and G. Y. Yeom, Appl. Phys. Lett. **86**, 052108 (2005).

[7] A. Khan, K. Balakrishnan, and T. Katona, Nat. Photonics **2**, 77 (2008).

[8] Y. Taniyasu, M. Kasu, and T. Makimoto, Nature (London) **441**, 325 (2006).

[9] S.-R. Jeon, Y.-H. Song, H.-J. Jang, G. M. Yang, S. W. Hwang, and S. J. Son, Appl. Phys. Lett. **78**, 3265 (2001).

[10] M. Diagne, Y. He, H. Zhou, E. Makarona, A. V. Nurmikko, J. Han, K. E. Waldrip, J. J. Figiel, and T. Takeuchi, Appl. Phys. Lett. **79**, 3720 (2001).

[11] C.-M. Lee, C.-C. Chuo, I.-L. Chen, J.-C. Chang, and J.-I. Chyi, IEEE Elec. Dev. Lett. **24**, 156 (2003).

[12] Y. X. Liu, D. Z.-Y. Ting, and T. C. McGill, Phys. Rev. B **54**, 5675 (1996).

[13] M. G. Burt, J. Phys.: Condens. Matter **4**, 6651 (1992).

[14] B. A. Foreman, Phys. Rev. B **48**, 4964 (1993).

[15] B. A. Foreman, Phys. Rev. B **56**, R12748 (1997).

[16] F. Bernardini, V. Fiorentini, and D. Vanderbilt, Phys. Rev. B **56**, R10024 (1997).

[17] I. Vurgaftman and J. R. Meyer, in *Nitride Semiconductor Devices: Principles and Simulation*, edited by J. Piprek (Wiley-CCH, Weinheim, 2007), pp. 13–48.

[18] T. Takeuchi, C. Wetzel, S. Yamaguchi, H. Sakai, H. Amano, I. Akasaki, Y. Kaneko, S. Nakagawa, Y. Yamaoka, and N. Yamada, Appl. Phys. Lett. **73**, 1691 (1998).

[19] S. Selberherr, *Analysis and Simulation of Semiconductor Devices* (Springer-Verlag, Berlin, 1984), pp. 175–181.

[20] J. Hader, J. V. Moloney, A. Thränhardt, and S. W. Koch, in *Nitride Semiconductor Devices: Principles and Simulation*, edited by J. Piprek (Wiley-CCH, Weinheim, 2007), pp. 145–167.

[21] S. L. Chuang and C. S. Chang, Phys. Rev. B **54**, 2491 (1996).

[22] R. G. Veprek, S. Steiger, and B. Witzigmann, Opt. Quantum Electron. (to be published).

[23] J. H. Wilkinson, *The Algebraic Eigenvalue Problem* (Oxford University Press, Oxford, 1965), pp. 633–634.

[24] Y. C. Chang and J. N. Schulman, Phys. Rev. B **25**, 3975 (1982).

[25] C. Y. Chao and S. L. Chuang, Phys. Rev. B **43**, 7027 (1991).

[26] M. Sweeny and J. Xu, Appl. Phys. Lett. **54**, 546 (1989).

[27] C. Rivas, R. Lake, W. Frensley, G. Klimeck, P. E. Thompson, K. D. Hobart, S. L. Rommel, and P. R. Berger, J. Appl. Phys. **94**, 5005 (2003).